Making ^{1}H-^{1}H couplings more accessible and accurate with selective 2DJ NMR experiments aided by ^{13}C satellites

François-Xavier Cantrelle,[1,2] Emmanuelle Boll[1,2] and Davy Sinnaeve[1,2]*

[1] CNRS, EMR9002 - Integrative Structural Biology, F-59000 Lille, France.

[2] Univ. Lille, Inserm, CHU Lille, Institut Pasteur de Lille, U1167 - RID-AGE - Risk Factors and Molecular Determinants of Aging-Related Diseases, F-59000 Lille, France.

* Corresponding author: davy.sinnaeve@univ-lille.fr

Supporting information

Table of Contents

1. Experimental

All NMR experiments were performed on a Bruker Avance III HD spectrometer operating at a ^{1}H and ^{13}C frequencies of 600.13 MHz and 150.90 MHz, respectively, equipped with a CP-QCI-F cryoprobe and running Topspin 3.6.2. All experiments were performed at 298.0 K. Pyridine (ca. 3.5 mM) was dissolved in D_2O, stachyose (6 mM) in D_2O, and norcamphor (2 mM) in DMSO-d6. A standard 5 mm sample tube was used for pyridine, a 5 mm Shigemi tube for Stachyose, and a standard 3 mm tube for norcamphor.

^{1}H-^{13}C HSQC experiments with sensitivity improved scheme and adiabatic ^{13}C decoupling were performed using standard pulse sequences from the Bruker library. ^{1}H-^{13}C CLIP-HSQC[1] spectra were performed using a standard Bruker HSQC pulse sequence that was adapted by omitting the ^{13}C composite pulse decoupling and by including a ^{13}C 90° hard pulse just before acquisition. For stachyose, spectral windows were 8.3315 ppm in F_2 and 49.9995 ppm in F_1, and the total number of complex time domain points were 4096 in F_2 and 512 in F_1. For norcamphor, spectral windows were 6.6652 ppm in F_2 and 70 ppm in F_1, and the total number of time domain points were 2048 in F_2 and 512 in F_1. Prior to Fourier transform, HSQC spectra were multiplied in both dimensions with a squared cosine bell function and zero filled until a 4096×2048 real data matrix size was obtained.

TSE-PSYCHE,[2] TSE-PSYCHEDELIC[3] spectra were performed using a 30 ms PSYCHE saltire shaped pulse and 40 ms 180° chirp pulses, each sweeping 10 kHz, applied during magnetic field gradients of 0.8025 G/cm. A PSYCHE flip angle of typically 15° was used. All pure shift and selective 2DJ experiments used a spectral window of 5000 Hz in the direct dimension. PSYCHEDELIC, SERFBIRD and SATASERF experiments typically used ISnob2 180° shaped inversion pulses and, in case of SATASERF, RSnob 180° shaped refocusing pulses.[4] All experiments using Interferogram pure shift acquisition had a time domain data chunk duration of 12.8 ms. Interferogram pure shift experiments were processed using the pshift au-program available from the University of Manchester NMR methodology group. All selective 2DJ data were multiplied with a Lorentz-to-Gauss resolution enhancement window function and zero filled before Fourier transform. For both interferogram and real-time pure shift selective 2DJ experiments (PSYCHEDELIC, SERFBIRD, SATASERF) where no ^{13}C chemical shift evolution was co-sampled with J_{HH}, an F_1 (2DJ dimension) reversed spectrum was added to the original. This improves the signal to noise ratio and, in combination with the Pell-Keeler method, reduces chunking artefacts.[3,5].

Spin density matrix calculations to obtain simulated spectra were performed in Matlab R2022b (The MathWorks, Inc.).

2. SERFBIRD and SATASERF pulse sequences

2.1 PFG amplitudes and phase cycles

Table S1: Phase cycle used for SERFBIRD (see Figure 4a in the main manuscript).

ϕ_1	02
ϕ_2	$0_4 2_4$
ϕ_3	$0_{16} 2_{16}$
ϕ_4	Echo: 3 Anti-echo: 1
ϕ_5	Echo: 3 + ϕ_0 Anti-echo: 1 + ϕ_0
ϕ_6	$0_2 1_2 0_2 1_2 2_2 3_2 2_2 3_2$
ϕ_7	$1_2 2_2 1_2 2_2 3_2 0_2 3_2 0_2$
ϕ_8	$2_2 3_2 2_2 3_2 0_2 1_2 0_2 1_2$
ϕ_R	$\phi_1 + 2\phi_3 - 2\phi_6$
$\phi_{9,n}$*	ϕ_n
$\phi_{10,n}$*	$1 + \phi_n$
$\phi_{11,n}$*	$2 + \phi_n$
ϕ_n* (supercycle)	0022 0220 2200 2002
ϕ_0	To obtain the $^{13}C^{\alpha}$ satellite: 0 To obtain the $^{13}C^{\beta}$ satellite: 2

* *n* is the index of the real-time pure shift acquisition loop as shown in Figure 4a.

Table S2. Phase cycle used for SATASERF (see Figure 4b in the main manuscript).

ϕ_1	02
ϕ_2	$0_2 2_2$
ϕ_3	$0_8 2_8$
ϕ_4	$0_4 1_4 0_4 1_4 2_4 3_4 2_4 3_4$
ϕ_R	$\phi_1 + 2\phi_3 - 2\phi_4$

Table S3: PFG amplitudes used for SERFBIRD and SATASERF, expressed as percentage of the maximum amplitude value (see Figure 4 in the main manuscript)

g_1	80%
g_2	-2.97%
g_3	17.13%
g_4	5.25%
g_5	44%
g_6	7.25%
g_7	13.17%
$g_{8,n}$*	For odd *n*: 17% For even *n*: 19%
$g_{9,n}$*	For odd *n*: 31% For even *n*: 33%

* *n* is the index of the real-time pure shift data acquisition loop shown in Figure 4.

2.2 Signal-to-noise comparisons

A standard 1D ^{1}H and the first increment (t_1 = 0) of SERFBIRD, SATASERF, with or without real-time BIRD homodecoupling, were recorded on the pyridine in D_2O sample. Identical acquisition times (0.683 s), spectral widths (3000 Hz), interscan relaxation delays (10 s), number of transients (32) and receiver gains were used. Ω_S-selective ISnob pulses (2.589 ms) were set to an empty region of the spectrum. The Ω_I-selective RSnob pulse (24.286 ms) in SATASERF was set to H4[$^{13}C^{\beta}$]. The INEPT and BIRD delays were matched to a $^{1}J_{CH}$ coupling of 171 Hz. Prior to Fourier transform, a squared cosine bell apodization function was used and the data was zero-filled until 262144 real spectrum data points. Baseline corrections were performed to regions used for signal and noise measurement prior to signal-to-noise calculation. The signal was measured on the H4[$^{13}C^{\beta}$] signal. This signal and the resulting signal-to-noise ratios are shown in Figure S1. Note that the pure shift version of SATASERF is most often run in interferogram mode rather than (BIRD) real-time decoupling (as discussed in section 2.4).

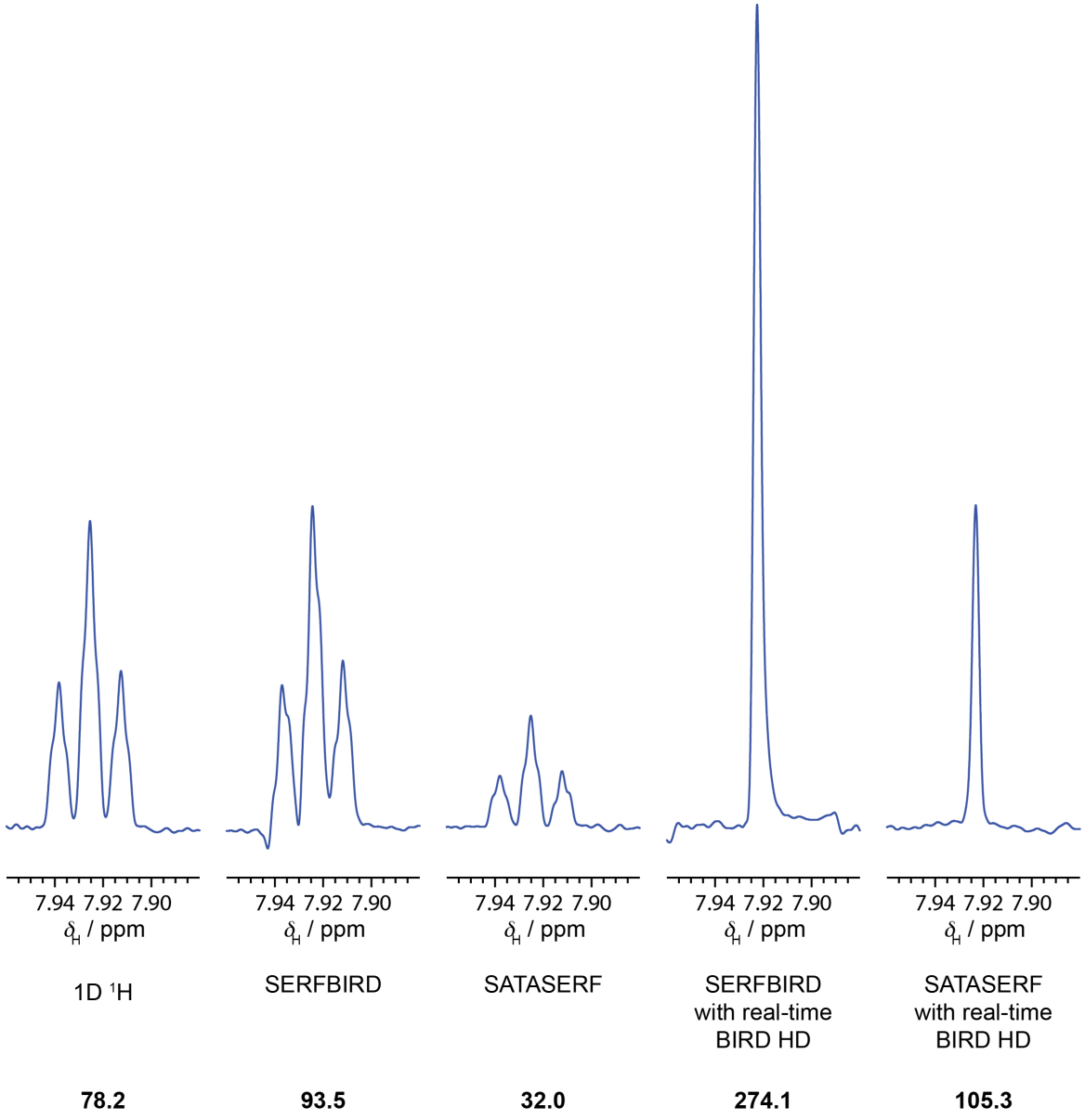

Figure S1: Signal-to-noise comparisons between the various experiments

2.3 Setup guidelines

The Bruker pulse sequence files are provided separately as supporting information, or upon request from the authors. These work with optional flags that need to be provided in the ZGOPTNS parameter, each time preceded by '-D'. For instance, activating the options 'CALC_SPH' and 'push_INT' requires the following input:

-DCALC_SPH -Dpush_INT

Table S4 shows an overview of the available flags.

Table S4. Overview of optional flags in the SERFBIRD / SATASERF pulse sequence codes.

Optional flag	SERFBIRD	SATASERF	Description
CALC_SPH	X	X	Automatic calculation of pulse lengths, power levels and offsets of the selective inversion pulses on spin S (and the selective refocusing ASR pulse in SATASERF) based on the user-provided chemical shift range and pulse shape bandwidth factors.
SEL13C	X	X	Use of a selective ^{13}C 180° refocusing pulse for spectral editing, and automatic pulse length and power level calculation for this pulse.
CH2suppr	X		Introduces an additional suppression step for $^{13}CH_2$ signals based on difference spectroscopy.
push_INT	X	X	Interferogram pure shift acquisition. Requires the experiment to be set up as a 3D experiment.
push_RT	X		Real-time BIRD pure shift acquisition.
push_RTBIRD		X	Real-time BIRD pure shift acquisition.
push_RTBASH		X	Real-time BASH pure shift acquisition.

Note that the push_INT, the push_RT, push_RTBIRD and push_RTBASH flags are all mutually exclusive, and should never be combined!

Except when the push_INT flag is enabled (see below), the experiment is a 2D experiment. The F1 dimension represents the selective 2DJ dimension, potentially mixed with ^{13}C chemical shift resolution. The observed nucleus in F1 should thus be set to ^{13}C. The FnMODE parameter in F1 should be set to Echo-Antiecho.

CNST15 controls co-sampling of J_{HH} and ^{13}C chemical shift evolutions. Set to 0, only J_{HH} evolution is sampled, meaning a pure selective 2DJ dimension is obtained. Set between 0 and 1, the indirect dimension encodes $J_{HH} + k*\Omega_{13C}$ evolution, with k = CNST15 and Ω_{13C} the ^{13}C offset from O2 in Hz. CNST15 thus downscales the ^{13}C chemical shift in this case. Set to 1

and above, the indirect dimension encodes $m*J_{HH} + \Omega_{13C}$ evolution, with m = CNST15. This means a full ^{1}H-^{13}C HSQC-type experiment is recorded, but with additional J_{HH} coupling evolution in F_1 that is upscaled by CNST15.

The O2 parameter should be set to the middle of the ^{13}C chemical shift region of the ^{13}C nuclei of interest, even if CNST15 is set to 0.

The Ω_S-selective inversion pulses are sp11 and sp12. Inversion type 180° pulse shapes such as ISnob or IBurp should be used. The shape in sp12 needs to be a time-reversed version of sp11, which can be created easily using the shape tool display in TopSpin. For this, open the desired inversion pulse, edit it using the 'time reversal' option and save it as a new shape. The offset in ppm of these pulses is set by CNST11.

For SERFBIRD, the selection of ^{13}C spin-state is controlled by the loop counter L2. Setting L2 to 1 delivers the $^{13}C^{\alpha}$ satellites, setting it to 0 delivers the $^{13}C^{\beta}$ satellites.

For SATASERF, the Ω_I-selective refocusing pulse is sp2. Refocusing type 180° pulses such as RSnob or REBurp should be used. The offset in ppm of this pulse is set by CNST18.

If the CALC_SPH flag is set:

The pulse lengths and power levels for all ^{1}H selective pulses (sp11, sp12, and sp2 in SATASERF) are conveniently calculated automatically, saving a lot of experimental setup time for the user.

The user provides the edges of the desired chemical shift region (in ppm) inverted by sp11 and sp12 in CNST6 and CNST7. The pulse length is calculated using the bandwidth factor (bwfac11) of the shaped pulse, and its power level based on the calibrated hard 90° pulse (P1) and power level (PLW1). The offset in CNST11 is automatically calculated.

For SATASERF, the user also provides the edges of the desired chemical shift region (in ppm) to be refocused by sp2 in CNST6 and CNST7. The pulse length is calculated using the bandwidth factor (bwfac2) of the shaped pulse, and its power level based on the calibrated hard 90° pulse (P1) and power level (PLW1). The offset in CNST18 is automatically calculated.

For safety reasons, it is advised to always verify the resulting pulse lengths and power levels before launching the experiments.

If the SEL13C flag is set:

Instead of a broadband ^{13}C refocusing 180° pulse, a bandselective ^{13}C refocusing 180° pulse is applied just before backtranfser to ^{1}H magnetization. As a consequence, only those protons bound to the selected ^{13}C nuclei will appear in the spectrum, providing a means for further spectral simplification. This presents an alternative to the co-sampling of ^{13}C chemical shift. The sp1 shaped pulse is used for this, and should be a refocusing 180° selective pulse such as RSnob or REBurp. The O2 parameter should be set to the middle of the selected ^{13}C region. The user defines the desired chemical shift bandwidth of the selective pulse in CNST28, from which the pulse length and power level is calculated based on the bandwidth factor of the pulse and the calibrated ^{13}C hard 90° pulse length (P3) and power level (PLW2).

If the CH2suppr flag is set:

In SERFBIRD, the ST2PT transfer in principle provides zero intensity for methylene protons, but in practice residual signals may remain if the $^{1}J_{CH}$ coupling mismatches the transfer delays used. Enabling this flag uses multiplicity editing and difference spectroscopy to further suppress these protons. For this, delays are used matched to a $^{1}J_{CH}$ coupling expected for the methylene groups, set in CNST5. Difference spectroscopy is performed using the F0 loop (td0 will be set to 2).

If the push_INT flag is set:

Interferogram pure shift acquisition is used. The experiment should be set as a 3D experiment with the selective 2DJ dimension now set in F2 (FnMODE = Echo-Antiecho) and the pure shift dimension in F1 (FnMODE = QF). The observed nucleus should be set to ^{13}C in F2, and ^{1}H in F1. TD in F1 corresponds to the number of chunks.

The number of time domain points per data chunk is set by the parameter L31. This should ideally be a power 2. The resulting chunk length will be displayed in the 'ChunkLength' parameter in the acquisition parameter summary screen in Topspin, and should ideally be 2 times the multiplet width. The use of L31 to define the chunk length is to ensure the time incrementation in the pseudo2D interferogram scheme is an exact multiple of the dwell time. For data processing using the Manchester pshift au-program, the SWH in F1 should still be set by hand to SWH in F3 divided by L31.

If the push_RT flag is set in SERFBIRD, or the push_RTBIRD or push_RTBASH flags in SATASERF:

Real-time pure shift acquisition is used. The experiment remains a 2D experiment. The number of chunks should be set using the L10 parameter. The resulting chunk length (D62 = AQ/L10) should ideally be 20-25 ms.

In SERFBIRD, real-time homodecoupling always applies the BIRD element. In case of SATASERF, either real-time BIRD or real-time BASH homodecoupling can be chosen.

2.4 Should interferogram or real-time homodecoupling be used?

Real-time homodecoupling is the fastest of both pure shift acquisition methods, but comers with the disadvantage of broadened line widths resulting from signal losses between the chunks of acquired time domain data. Interferogram acquisition thus always delivers the most superior resolution of the two. The question, therefore, is how much line broadening the real-time homodecoupling induces.

BASH (a.k.a. HOBS) real-time homodecoupling works well only if the selective 180° pulse can be chosen sufficiently short (preferably much shorter than the chunk durations) in order to limit T_2 signal losses.[6] If this cannot be achieved, interferogram acquisition should be preferred. As the ^{13}C BIRD element is relatively short, signal losses by relaxation are limited, usually leading to marginally broader singlet line widths in real-time experiments compared to interferogram acquisition.[7] This makes BIRD real-time homodecoupling preferable over BIRD interferogram in most cases. One notable exception is when the BIRD element itself is imperfect due to its delays being significantly mismatched with the actual ^{1}H-^{13}C one-bond coupling or due to ^{1}H-^{1}H coupling evolution during these delays.[7] This can be the case under molecular alignment conditions (*cf.*, measurement of residual dipolar couplings) where there exists a wide range of ^{1}H-^{13}C and ^{1}H-^{1}H RDCs.[3,8] Under such circumstances, interferogram acquisition might be preferred.

For SERFBIRD, real-time BIRD homodecoupling is thus nearly always preferred. In contrast, SATASERF is primarily intended to detect CH_2 proton signals that feature a $^{2}J_{HH}$ splitting, which BIRD homodecoupling does not remove. This leads to imperfect pure shift resolution. Although real-time BIRD homodecoupling is provided in the SATASERF pulse sequence code, in most cases it is thus not the best choice. An exception is when the protons in the CH_2 group are fully chemically shift degenerate (for instance, when they are enantiotopic), or for methyl signals. In these cases, under isotropic conditions (*i.e.*, without geminal dipolar couplings present), the $^{2}J_{HH}$ couplings are absent from the spectrum and BIRD homodecoupling will thus deliver full pure shift resolution.

For SATASERF, an alternative is BASH real-time homodecoupling. Given the purpose of the experiment is to focus on a ^{13}C satellite when the ^{12}C isotopomer signal is strongly coupled to another proton, selective 180° refocusing pulses with narrow bandwidths will typically need to be used to avoid irradiating this nearby ^{1}H coupling partner. Successful BASH homodecoupling thus most often requires long selective pulses, anathema for real-time pure shift acquisition. This implies interferogram (BASH) pure shift acquisition will most often be the preferred choice for pure shift acquisition in SATASERF.

If real-time pure shift acquisition can be used, but the ^{13}C satellite multiplet is already well-resolved without pure shift resolution, it nevertheless can still be beneficial to apply it, as usually the signal-to-noise ratio per unit experimental time will increase as a result (see section 2.2). If pure shift resolution is not needed and only interferogram acquisition would provide acceptable line widths, the non-pure shifted experiment might be the better option.

To summarize:

- For methine (CH) groups, usually the best results are obtained with SERFBIRD applying BIRD real-time homodecoupling, even when pure shift resolution is not absolutely required.

- For methylene (CH_2) groups with protons that are not chemical shift degenerate, SATASERF has to be used. If pure shift resolution is required to resolve the signal, then the best results are typically obtained with interferogram pure shift acquisition.
- For methylene (CH_2) groups with protons having degenerate chemical shifts or for methyl (CH_3) groups, the ST2PT sequence in SERFBIRD will not function properly due to more than one $^{1}J_{CH}$ coupling being active on the ^{13}C nucleus. Therefore, SATASERF still needs to be used, but real-time BIRD pure shift resolution will likely be preferred.
- Under anisotropic conditions, one needs to take into account the impact of having a wide variety of $^{1}T_{CH}$ total couplings, large and abundant $^{n}T_{HH}$ total couplings and, in case of chemical shift degenerate methylene and methyl groups, $^{2}D_{HH}$ dipolar couplings. All of these may significantly affect the performance of the ST2PT sequence and BIRD or BASH homodecoupling.

3. A note on ^{13}C satellites and measurement at multiple magnetic fields

In exceptional cases, it could turn out that the parent *all*-^{12}C isotopomer signal and both ^{13}C satellites are each separately involved in a strong coupling interaction. Then no selective 2DJ experiment would be free of the complications from strong coupling. A way to circumvent this would be to switch to a different magnetic field. It turns out that strong coupling between a ^{13}C satellite and a ^{12}C-bound proton fades much more quickly upon a change in magnetic field strength than does strong coupling involving two ^{12}C-bound protons.

The frequency difference between two protons A and B linearly increases with B_0 with a slope proportional to the difference in chemical shift: $\Delta\nu_{AB} \propto \Delta\delta_{AB}B_0$. For strongly coupled protons in the *all*-^{12}C isotopomer, the difference in chemical shift is by definition small and close to zero, meaning a very large or even an unrealistic increase in B_0 would be needed to lift the strong coupling condition. Figure S2a shows simulated spectra for an ABX ^{1}H spin system at 600 MHz (ν_A = –8.0 Hz, ν_B = 8.0 Hz, ν_X = 800.0 Hz, J_{AB} = 12.0 Hz, J_{AX} = 9.0 Hz, J_{BX} = 4.0 Hz). The spectra in Figures S2b and S2c show the same spin system at 900 MHz and 1200 MHz, respectively. It is clear that a large change in magnetic field strength is required to alleviate the strong coupling.

Figure S2d-f show simulated spectra for an ABX ^{1}H spin system at 600 MHz, 900 MHz and 1200 MHz, respectively, but in this case with A experiencing a $^1J_{CH}$ coupling. At 600 MHz, the spectral parameters are: ν_A = –80.5 Hz, ν_B = 8.0 Hz, ν_X = 800.0 Hz, J_{AB} = 12.0 Hz, J_{AX} = 9.0 Hz, J_{BX} = 4.0 Hz and J_{CAHA} = 145.0 Hz. At 600 MHz, the HA[^{13}C$^{\alpha}$] satellite ends up at –8.0 Hz, meaning it is strongly coupled with HB[^{12}C] to the same degree as was the case in Figure S2a. Because $^1J_{CAHA}$ is field-independent and the actual chemical shift difference between A and B is much larger than in the previous simulation, HA[^{13}C$^{\alpha}$] moves away from HB[^{12}C] much more rapidly upon increasing magnetic field strength (Figure S2e-f). Within the range of currently available magnetic field strengths for NMR spectroscopy, it should thus be feasible to sufficiently lift the degree of strong coupling. With SATASERF/SERFBIRD experiments, strong coupling conditions can thus be further avoided by making good use of different magnetic fields.

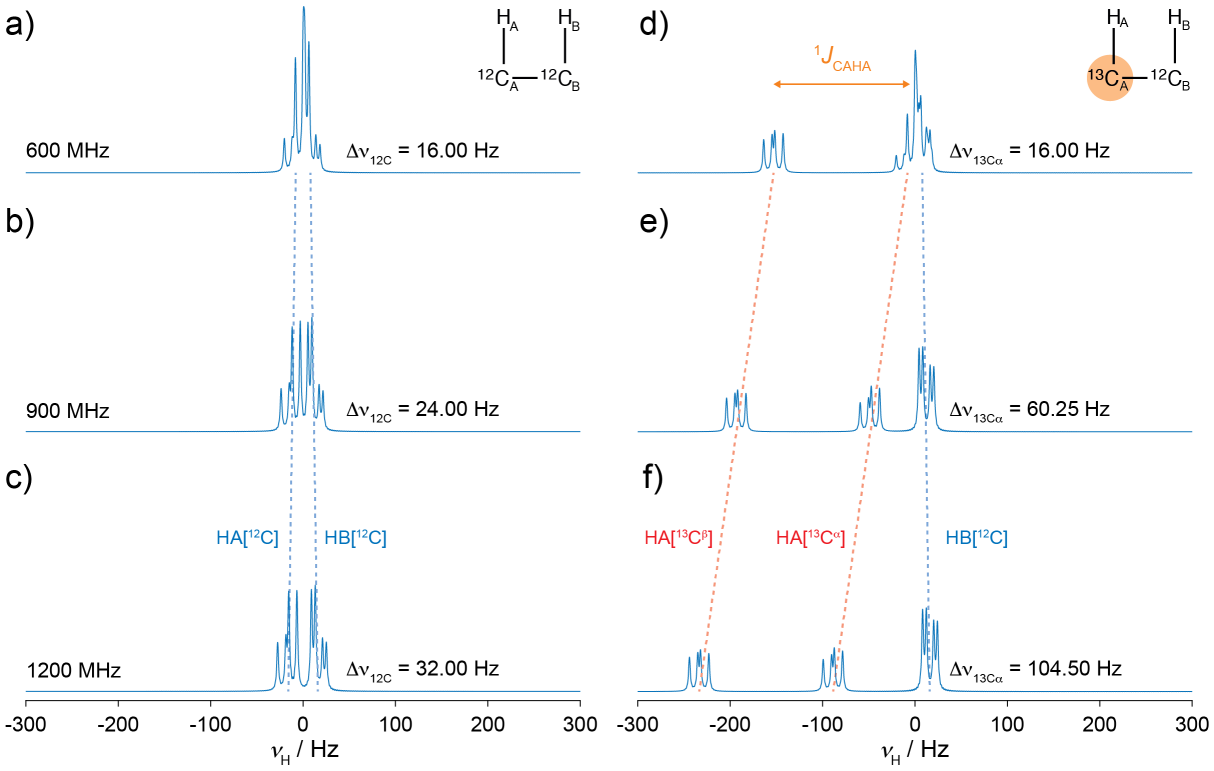

Figure S2: Simulated 1D ^{1}H spectra of an ABX ^{1}H spin system at (a) 600 MHz, (b) 900 MHz and (c) 1200 MHz, and of an ABX ^{1}H spin system with A experiencing a $^1J_{CH}$ coupling at (d) 600 MHz, (e) 900 MHz and (f) 1200 MHz. See text for spectral parameter values.

4. NMR data for Stachyose

4.1 NMR assignment

The assignment of stachyose (Figure S3) is shown in Figure S4 on a multiplicity edited ^{1}H-^{13}C HSQC: signals from CH groups are positive (black) and from CH_2 groups are negative (red). Strongly coupled vicinal proton pairs are indicated.

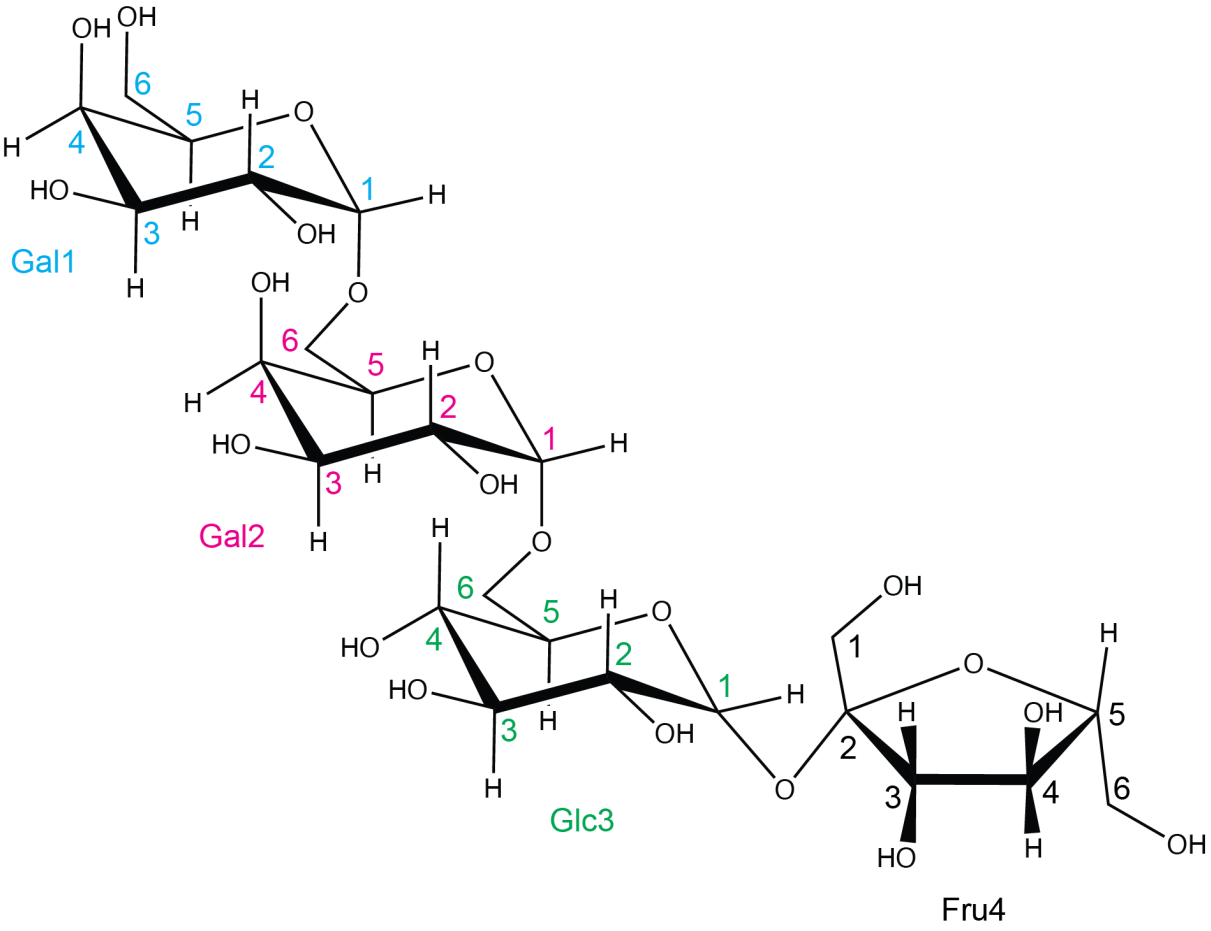

Figure S3: Structure of Stachyose.

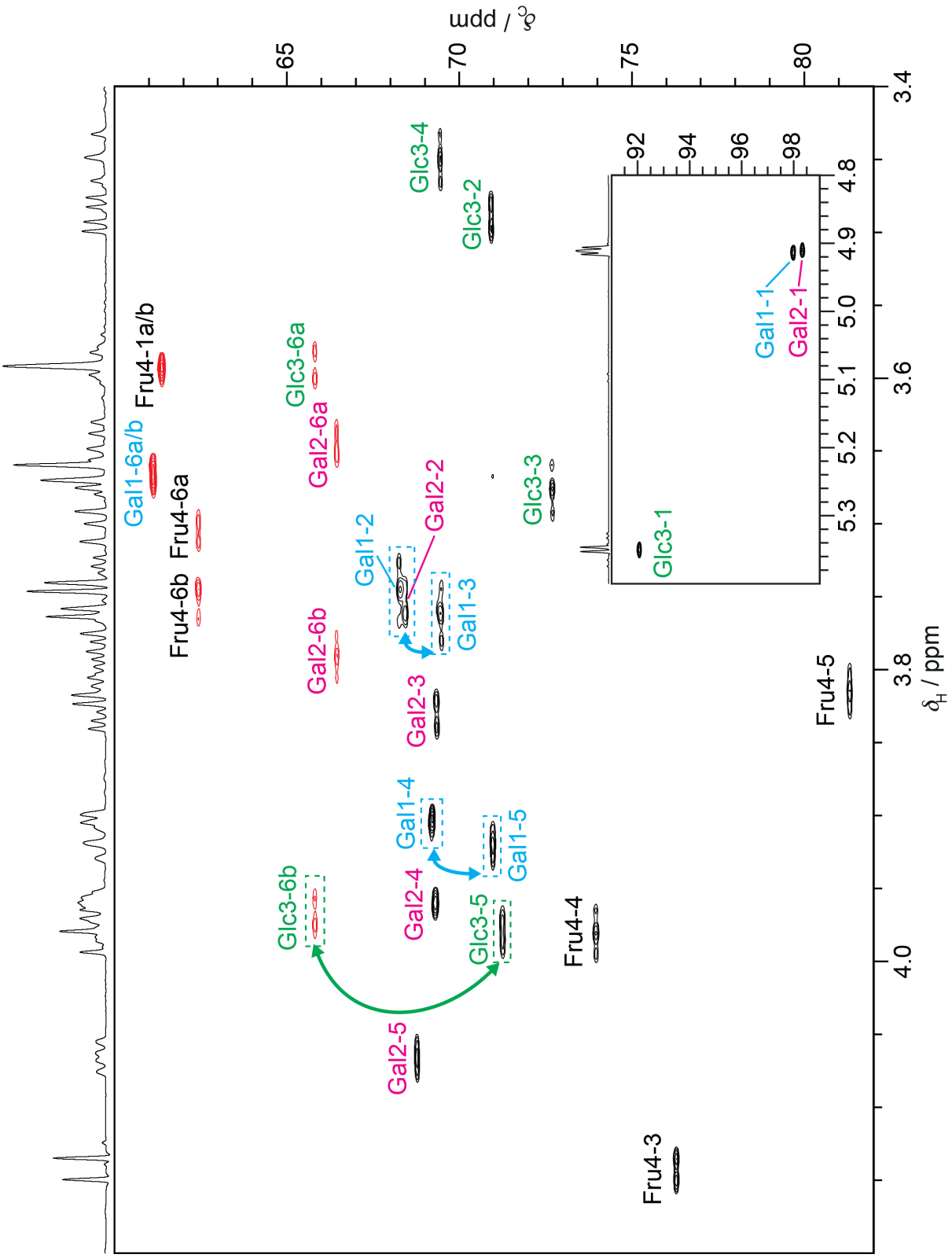

Figure S4: Multiplicity edited ^{1}H-^{13}C HSQC of stachyose, acquired using ^{13}C decoupling, showing the assignment and indicating strongly coupled ^{1}H pairs.

4.2 Overview of selective 2DJ experiments

Experimental data can be downloaded from: http://dx.doi.org/10.5281/zenodo.10473716

Table S5: PSYCHEDELIC experiments performed on stachyose.

Label	Experiment number	Ω_S region / ppm	Selected protons S	Couplings extracted
P1	1010	4.025-4.19	**Gal2:** H5 **Fru4:** H3	**Gal2:** H4-H5, H6a-H5, H6b-H5 **Fru4:** H4-H3
P2	1011	3.942-4.01	**Gal2:** H4 **Glc3:** H5, H6b **Fru4:** H4	**Gal2:** H3-H4, H5-H4 **Glc3:**[a] H4-H5[b] **Fru4:** H3-H4, H5-H4
P3	1012	3.88-3.94	**Gal1:** H4, H5	**Gal1:**[c] H3-H4[d]
P4	1014	3.788-3.849	**Gal2:** H3, H6b **Fru4:** H5	**Gal2:** H2-H3, H4-H3, H6a-H6b, H5-H6b **Fru4:** H4-H5, H6a-H5, H6b-H5
P5	1015	3.6172-3.7188	**Gal1:** H6a, H6b **Gal2:** H6a **Glc3:** H3 **Fru4:** H6a	**Gal2:** H5-H6a, H6b-H6a **Glc3:** H2-H3, H4-H3 **Fru4:** H5-H6a, H6b-H6a
P6	1016	3.55-3.6166	**Glc3:** H6a **Fru4:** H1a, H1b	**Glc3:**[e] H6b-H6a[b]
P7	1022	4.8-5.5	**Gal1:** H1 **Gal2:** H1 **Glc3:** H1	**Gal1:** H2-H1[f] **Gal2:** H2-H1 **Glc3:** H2-H1

[a] Both H6a-H5 and H6a-H6b couplings not resolvable on H6a due to doublet of doublet response and the overlap with Fru4-H1a/H1b signal.
[b] Splitting affected by strong coupling between Glc3 H5 and H6b.
[c] Individual Gal-1 H6a-H5 and H6b-H5 couplings not measurable due to chemical shift degeneracy of H6a and H6b protons.
[d] Splitting affected by strong coupling between Gal1 H2 and H3 and H4 and H5.
[e] H6a-H5 not measured due to overlap of Glc3 H5 signal with Fru4 H4.
[f] Splitting affected by strong coupling between Gal1 H2 and H3.

Table S6: SERFBIRD experiments performed on stachyose

Label	Expno	^{13}C spin-state	Ω_S region / ppm	Selected protons	Couplings extracted
SB1	20	$^{13}C^{\alpha}$	3.71-3.788	**Gal1:** H2[^{12}C], H3[^{12}C] **Gal2:** H2[^{12}C], H6b[^{12}C]	**Gal1:**[a],[b] H2[$^{13}C^{\alpha}$]-H3[^{12}C] H3[$^{13}C^{\alpha}$]-H2[^{12}C] **Gal2**[a],[c],[d],[e]
SB2	21	$^{13}C^{\beta}$	3.945-4.007	**Gal2:** H4[^{12}C] **Glc3:** H5[^{12}C], H6b[^{12}C] **Fru4:** H4[^{12}C]	**Gal2:**[f] H5[$^{13}C^{\beta}$]-H4[^{12}C] **Glc3:** H4[$^{13}C^{\beta}$]-H5[^{12}C][g] H5[$^{13}C^{\beta}$]-H6b[^{12}C][h] **Fru4:**[i] H3[$^{13}C^{\beta}$]-H4[^{12}C]
SB3	22	$^{13}C^{\beta}$	3.56-3.62	**Glc3:** H6a[^{12}C]	**Glc3:** H5[$^{13}C^{\beta}$]-H6a[^{12}C][h]
SB4	23	$^{13}C^{\beta}$	3.42-3.473	**Glc3:** H4[^{12}C]	**Glc3:**[j] H5[$^{13}C^{\beta}$]-H4[^{12}C]
SB5	24	$^{13}C^{\beta}$	3.71-3.788	**Gal1:** H2[^{12}C], H3[^{12}C] **Gal2:** H2[^{12}C], H6b[^{12}C]	**Gal1:**[ax] H2[$^{13}C^{\beta}$]-H3[^{12}C] H3[$^{13}C^{\beta}$]-H2[^{12}C][l] H4[$^{13}C^{\beta}$]-H3[^{12}C][m] **Gal2:**[a] H3[$^{13}C^{\beta}$]-H2[^{12}C][f] H5[$^{13}C^{\beta}$]-H6b[^{12}C]
SB6	25	$^{13}C^{\alpha}$	3.88-3.94	**Gal1:** H4[^{12}C], H5[^{12}C]	**Gal1:** H4[$^{13}C^{\alpha}$]-H5[^{12}C][n] H5[$^{13}C^{\alpha}$]-H4[^{12}C] H3[$^{13}C^{\alpha}$]-H4[^{12}C]
SB7	26	$^{13}C^{\alpha}$	4.7-5.5	**Gal1:** H1[^{12}C] **Gal2:** H1[^{12}C] **Glc3:** H1[^{12}C]	**Gal1:** H2[$^{13}C^{\alpha}$]-H1[^{12}C] **Gal2:** H2[$^{13}C^{\alpha}$]-H1[^{12}C] **Glc3:** H2[$^{13}C^{\alpha}$]-H1[^{12}C]
SB8[o]	29	$^{13}C^{\beta}$	3.56-3.62	**Glc3:** H6a[^{12}C]	**Glc3:** H5[$^{13}C^{\beta}$]-H6a[^{12}C]
SB9	33	$^{13}C^{\beta}$	3.88-3.94	**Gal1:** H4[^{12}C], H5[^{12}C]	**Gal1:**[p] H5[$^{13}C^{\alpha}$]-H4[^{12}C] H4[$^{13}C^{\alpha}$]-H5[^{12}C]

Label	Expno	^{13}C spin-state	Ω_S region / ppm	Selected protons	Couplings extracted
SB10[o]	34	$^{13}C^{\beta}$	3.945-4.007	**Gal2:** H4[^{12}C] **Glc3:** H5[^{12}C], H6b[^{12}C] **Fru4:** H4[^{12}C]	**Glc3:** H5[$^{13}C^{\beta}$]-H6b[^{12}C]

[a] Gal1 and Gal2 H1[$^{13}C^{\alpha}$]-H2[^{12}C] couplings could not be extracted from this experiment due to overlap between the Gal1 H1[$^{13}C^{\alpha}$] and Gal2 H1[$^{13}C^{\alpha}$].
[b] Gal1 H4[$^{13}C^{\alpha}$] signal falls within the Ω_S region and is thus not observed.
[c] Gal2 H3[$^{13}C^{\alpha}$] signal falls within the Ω_S region and is thus not observed.
[d] Gal2 H4[$^{13}C^{\alpha}$] is strongly coupled with H3[^{12}C], remarkably resulting in a splitting in F_1 on this signal due to the H2-H3 coupling.
[e] Gal2 H5[$^{13}C^{\alpha}$] is strongly coupled with H4[^{12}C], and the H5[$^{13}C^{\alpha}$]-H6b[^{12}C] coupling was therefore not extracted.
[f] Splitting affected by strong coupling between Gal2 H3[$^{13}C^{\beta}$] and H4[^{12}C].
[g] Splitting affected by strong coupling between Glc3 H5[^{12}C] and H6b[^{12}C].
[h] Coupling could not be extracted due to peak overlap with Fru4 H4[$^{13}C^{\beta}$].
[i] H5[$^{13}C^{\beta}$] signal falls within the Ω_S region and is thus not observed.
[j] Glc3 H3[$^{13}C^{\beta}$] signal falls within the Ω_S region and is thus not observed.
[k] Gal1 and Gal2 H1[$^{13}C^{\beta}$]-H2[^{12}C] couplings could not be extracted from this experiment due to overlap between the Gal1 H1[$^{13}C^{\beta}$] and Gal2 H1[$^{13}C^{\beta}$].
[l] Splitting affected by strong coupling between Gal1 H3[$^{13}C^{\beta}$] and H4[^{12}C].
[m] Splitting affected by strong coupling between Gal1 H2[^{12}C] and H3[^{12}C].
[n] Splitting affected by strong coupling between Gal1 H4[$^{13}C^{\alpha}$] and H3[^{12}C].
[o] Measured with ^{13}C chemical shift evolution sampled during t_1, with k = 0.025.
[p] Gal1 H3[$^{13}C^{\beta}$] signal falls within the Ω_S region and is thus not observed.

Table S7: SATASERF experiments performed on stachyose.

Label	Expno	Ω_I region / ppm	Observed signals	Ω_S region / ppm	Selected protons	Couplings extracted
SS1	1004	4.03-4.15	**Gal1:** H4[$^{13}C^{\beta}$] H5[$^{13}C^{\beta}$] **Gal2:** H4[$^{13}C^{\beta}$] **Glc3:** H5[$^{13}C^{\beta}$] H6b[$^{13}C^{\beta}$] **Fru4:** H3[$^{13}C^{\alpha}$] H4[$^{13}C^{\beta}$]	3.546-3.74	**Gal1:** H6a[^{12}C] H6b[^{12}C] **Glc3:** H6a[^{12}C] H6a[$^{13}C^{\beta}$] H3[^{12}C] **Fru1:** H1a,b[^{12}C] H6a[^{12}C]	**Glc3:** H6b[$^{13}C^{\beta}$]-H6a[$^{13}C^{\beta}$] H5[$^{13}C^{\beta}$]-H6a[^{12}C][a]

[a] Coupling could not be extracted due to overlap between Glc3 H5[$^{13}C^{\beta}$] and Fru4 H4[$^{13}C^{\beta}$]

4.3 SATASERF experiment to measure Glc3 H6a-H6b

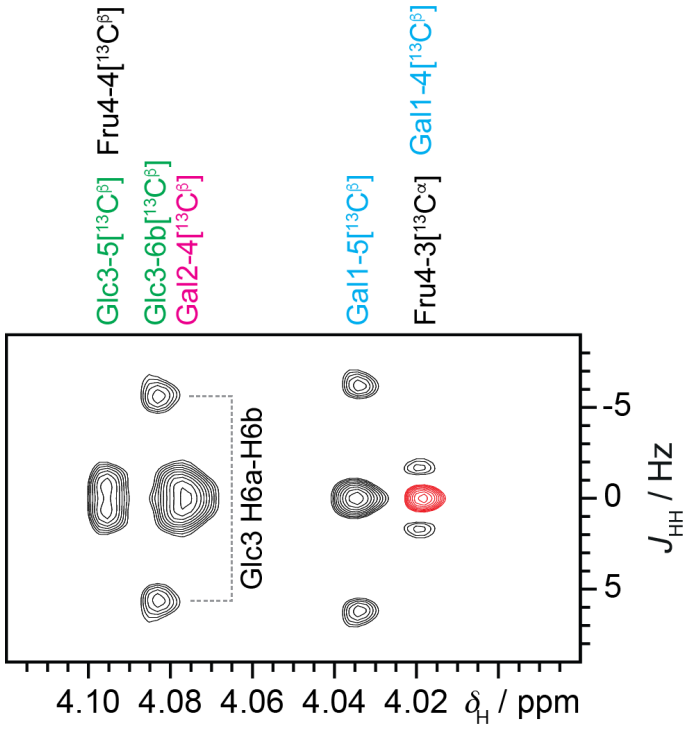

Figure S5: SATASERF experiment on stachyose (SS1 in Table S7) to measure the Glc3 H6a-H6b geminal *J*-coupling on the H6b[$^{13}C^{\beta}$] signal to avoid the Glc3 H5-H6b strong coupling in the *all*-^{12}C isotopomer. Assignments of the other signals are shown on top.

4.4 Coupling data

The Gal1 (H6a,H6b) and Fru (H1a,H1b) geminal proton pairs are chemical shift degenerate, implying that no individual coupling data between and to them could be extracted.

Table S8: *J*-coupling data for stachyose.

Values affected by the effects of strong coupling are shown in red.
*Strongly coupled protons in the all-^{12}C isotopomer are shaded **pink**.*
Previously reported J-coupling values by McIntyre and Vogel are shown.[9] These were reported with just 1 Hz precision. Values deviating by more than 1 Hz are shaded in green.

Coupling partners		J / Hz					
		PSYCHEDELIC		SERFBIRD/SATASERF		Final coupling	McIntyre
Galactose-1							
H1	H2	3.6[a] P7	--	4.0 SB7	--	**4.0**	4
H2	**H3**	--	--	10.2 / 10.3 SB1	10.3 / 9.2[b] SB5	**10.3**	10
H3	H4	3.2[c] P3	--	3.1[d] SB5	3.5 SB6	**3.5**	3
H4	**H5**	--	--	1.2 / 0.9[e] SB6	1.2 / 1.2 SB9	**1.2**	1
Galactose-2							
H1	H2	3.9 P7	--	4.0 SB7	--	**4.0**	4
H2	H3	10.4 P4	--	12.4[f] SB5	--	**10.4**	10
H3	H4	3.4 P2	3.4 P4	--	--	**3.4**	3
H4	H5	1.3 P1	1.3 P2	1.3 SB2	--	**1.3**	1
H5	H6a	4.7 P1	4.7 P5	--	--	**4.7**	5
H5	H6b	7.7 P1	7.6 P4	7.6 SB5	--	**7.6**	8
H6a	H6b	10.9 P4	10.8 P5	--	--	**10.9**	11
Glucose-3							
H1	H2	3.9 P7	--	3.9 SB7	--	**3.9**	4

Coupling partners		J / Hz					
		PSYCHEDELIC		SERFBIRD/SATASERF		Final coupling	McIntyre
H2	H3	10.0 P5	--	--	--	**10.0**	10
H3	H4	9.2 P5	--	--	--	**9.2**	9
H4	H5	10.0[g] P2	--	10.0[h] SB2	10.2 SB4	**10.2**	10
H5	H6a	--	--	1.9 SB8	--	**1.9**	9
H5	**H6b**	--	--	4.1 SB10	--	**4.1**	4
H6a	H6b	11.4[g] P6	--	11.3 SS1	--	**11.3**	13
Fructose-4							
H3	H4	8.8 P1	8.8 P2	8.9 SB2	--	**8.8**	9
H4	H5	8.5 P2	8.5 P4	--	--	**8.5**	9
H5	H6a	7.3 P4	7.2 P5	--	--	**7.3**	7
H5	H6b	3.0 P4	--	--	--	**3.0**	4
H6a	H6b	12.0 P5	--	--	--	**12.0**	12

[a] Splitting affected by strong coupling between Gal1 H2[^{12}C] and H3[^{12}C].
[b] Splitting affected by strong coupling between Gal1 H3[$^{13}C^{\beta}$] and H4[^{12}C].
[c] Splitting affected by strong coupling between Gal1 H2[^{12}C] and H3[^{12}C] and H4[^{12}C] and H5[^{12}C].
[d] Splitting affected by strong coupling between Gal1 H2[^{12}C] and H3[^{12}C].
[e] Splitting affected by strong coupling between Gal1 H4[$^{13}C^{\alpha}$] and H3[^{12}C].
[f] Splitting affected by strong coupling between Gal2 H3[$^{13}C^{\beta}$] and H4[^{12}C].
[g] Splitting affected by strong coupling between Glc3 H5[^{12}C] and H6b[^{12}C].
[h] Splitting affected by strong coupling between Glc3 H5[^{12}C] and H6b[^{12}C].

5. NMR data for norcamphor

5.1 NMR spectra and assignment

The assignment of norcamphor (Figure S6) is shown on a ^{1}H-^{13}C HSQC in Figure S7. Strongly coupled proton pairs are indicated.

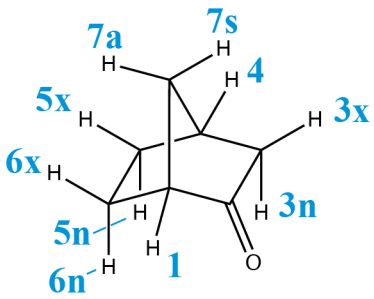

Figure S6: Structure of norcamphor.

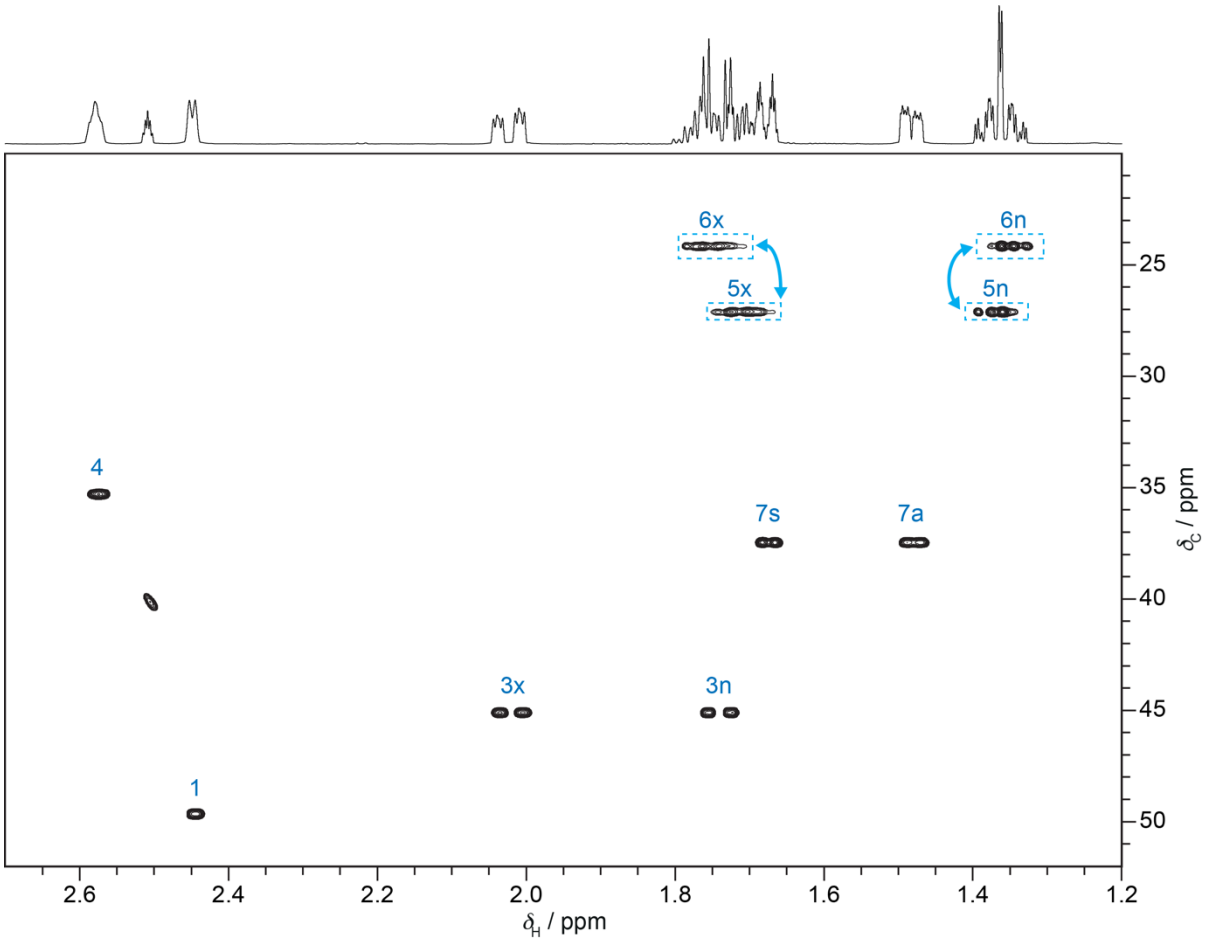

Figure S7: ^{1}H-^{13}C HSQC of norcamphor, acquired using ^{13}C decoupling, showing the assignment and indicating strongly coupled ^{1}H pairs.

5.2 Overview of selective 2DJ experiments

Experimental data can be downloaded from: http://dx.doi.org/10.5281/zenodo.10473716

Table S9: PSYCHEDELIC experiments performed on norcamphor.

Label	Experiment number	Ω_S region / ppm	Selected protons	couplings
P1	1013	2.4-2.5	1	3x-1 4-1 6x-1 7a-1 7s-1
P2	1021	1.43-1.53	7a	1-7a 3n-7a 4-7a 7s-7a
P3	1022	1.90-2.10	3x	1-3x 3n-3x 4-3x 5x-3x 6x-3x
P4	1040	2.5-2.6	4	1-4 3x-4 5x-4 7s-4 7a-4

Table S10: SERFBIRD experiments performed on norcamphor.

Label	Expno	^{13}C spin-state	Ω_S region / ppm	Selected protons	Couplings extracted
SB1	21	$^{13}C^{\beta}$	2.4-2.5	1[^{12}C]	H4[$^{13}C^{\beta}$]-H1[^{12}C]
SB2	32	$^{13}C^{\beta}$	1.95-2.10	3x[^{12}C]	H1[$^{13}C^{\beta}$]-H3x[^{12}C] H4[$^{13}C^{\beta}$]-H3x[^{12}C]

Table S11: SATASERF experiments performed on norcamphor.

Label	Expno	Ω_I region / ppm	Observed signals	Ω_S region / ppm	Selected protons	Couplings extracted
SS1	A/1005	1.415-1.525	5n[$^{13}C^{\beta}$] 6n[$^{13}C^{\beta}$]	1.308-1.410	5n[^{12}C] 6n[^{12}C]	5n[$^{13}C^{\beta}$]-6n[^{12}C] 6n[$^{13}C^{\beta}$]-5n[^{12}C]
SS2	A/1006	1.18-1.303	5n[$^{13}C^{\alpha}$] 6n[$^{13}C^{\alpha}$]	1.308-1.410	5n[^{12}C] 6n[^{12}C]	5n[$^{13}C^{\alpha}$]-6n[^{12}C] 6n[$^{13}C^{\alpha}$]-5n[^{12}C]
SS3	A/1009	1.415-1.525	5n[$^{13}C^{\beta}$] 6n[$^{13}C^{\beta}$]	1.84-1.913	6x[$^{13}C^{\beta}$]	6n[$^{13}C^{\beta}$]-6x[$^{13}C^{\beta}$]
SS4	A/1010	1.18-1.303	5n[$^{13}C^{\alpha}$] 6n[$^{13}C^{\alpha}$]	1.55-1.64	5x[$^{13}C^{\alpha}$]	5n[$^{13}C^{\alpha}$]-5x[$^{13}C^{\alpha}$]
SS5	A/1011	1.84-1.913	6x[$^{13}C^{\beta}$]	1.308-1.410	5n[^{12}C] 6n[^{12}C]	6x[$^{13}C^{\beta}$]-5n[^{12}C]
SS6	A/1012	1.55-1.64	5x[$^{13}C^{\alpha}$]	1.308-1.410	5n[^{12}C] 6n[^{12}C]	5x[$^{13}C^{\alpha}$]-6n[^{12}C]
SS7	A/1014	1.84-1.913	6x[$^{13}C^{\beta}$]	2.4-2.5	1[^{12}C]	6x[$^{13}C^{\beta}$]-1[^{12}C]
SS8	A/1015	1.55-1.64	5x[$^{13}C^{\alpha}$]	2.5-2.6	4[^{12}C]	5x[$^{13}C^{\alpha}$]-4[^{12}C]
SS9	A/1016	1.55-1.64	5x[$^{13}C^{\alpha}$]	1.9-2.1	3x[^{12}C]	5x[$^{13}C^{\alpha}$]-3x[^{12}C]
SS10	A/1019	1.415-1.525	5n[$^{13}C^{\beta}$] 6n[$^{13}C^{\beta}$]	1.64-1.70	7s[^{12}C]	5n[$^{13}C^{\beta}$]-7s[^{12}C]
SS11	A/1032	1.84-1.913	6x[$^{13}C^{\beta}$]	2.5-2.6	4[^{12}C]	6x[$^{13}C^{\beta}$]-4[^{12}C]
SS12	A/1033	1.415-1.525	5n[$^{13}C^{\beta}$] 6n[$^{13}C^{\beta}$]	2.5-2.6	4[^{12}C]	5n[$^{13}C^{\beta}$]-4[^{12}C] 6n[$^{13}C^{\beta}$]-4[^{12}C]
SS13	A/1034	1.415-1.525	5n[$^{13}C^{\beta}$] 6n[$^{13}C^{\beta}$]	2.4-2.5	1[^{12}C]	5n[$^{13}C^{\beta}$]-1[^{12}C] 6n[$^{13}C^{\beta}$]-1[^{12}C]
SS14	A/1035	1.18-1.303	5n[$^{13}C^{\alpha}$] 6n[$^{13}C^{\alpha}$]	2.5-2.6	4[^{12}C]	5n[$^{13}C^{\alpha}$]-4[^{12}C] 6n[$^{13}C^{\alpha}$]-4[^{12}C]
SS15	A/1036	1.18-1.303	5n[$^{13}C^{\alpha}$] 6n[$^{13}C^{\alpha}$]	2.4-2.5	1[^{12}C]	5n[$^{13}C^{\alpha}$]-1[^{12}C] 6n[$^{13}C^{\alpha}$]-1[^{12}C]
SS16	A/1037	1.53-1.63	7a[$^{13}C^{\beta}$] 7s[$^{13}C^{\alpha}$]	2.5-2.6	4[^{12}C]	7a[$^{13}C^{\beta}$]-4[^{12}C] 7s[$^{13}C^{\alpha}$]-4[^{12}C]
SS17	A/1038	1.53-1.63	7a[$^{13}C^{\beta}$] 7s[$^{13}C^{\alpha}$]	2.4-2.5	1[^{12}C]	7a[$^{13}C^{\beta}$]-1[^{12}C] 7s[$^{13}C^{\alpha}$]-1[^{12}C]
SS18	B/1023	1.84-1.913	6x[$^{13}C^{\beta}$]	1.9-2.1	3x[^{12}C]	6x[$^{13}C^{\beta}$]-3x[^{12}C]
SS19	B/1024	1.84-1.913	6x[$^{13}C^{\beta}$]	1.64-1.70	7s[^{12}C]	6x[$^{13}C^{\beta}$]-7s[^{12}C]
SS20	B/1025	1.18-1.303	5n[$^{13}C^{\alpha}$] 6n[$^{13}C^{\alpha}$]	1.43-1.53	7a[^{12}C]	5n[$^{13}C^{\alpha}$]-7a[^{12}C][a] 6n[$^{13}C^{\alpha}$]-7a[^{12}C][a]
SS21	C/1022	1.55-1.64	5x[$^{13}C^{\alpha}$]	1.64-1.70	7s[^{12}C]	5x[$^{13}C^{\alpha}$]-7s[^{12}C][a]
SS22	C/1024	1.82-1.95	3x[$^{13}C^{\alpha}$] 3n[$^{13}C^{\beta}$]	2.5-2.6	4[^{12}C]	3x[$^{13}C^{\alpha}$]-4[^{12}C] 3n[$^{13}C^{\beta}$]-4[^{12}C]
SS23	C/1025	1.82-1.95	3x[$^{13}C^{\alpha}$] 3n[$^{13}C^{\beta}$]	1.64-1.69	7s[^{12}C] 3n[$^{13}C^{\alpha}$][b]	3n[$^{13}C^{\beta}$]-7s[^{12}C][a] 3x[$^{13}C^{\alpha}$]-3n[$^{13}C^{\alpha}$][b]
SS24	C/1028	1.18-1.303	5n[$^{13}C^{\alpha}$] 6n[$^{13}C^{\alpha}$]	1.9-2.1	3x[^{12}C]	5n[$^{13}C^{\alpha}$]-3x[^{12}C] 6n[$^{13}C^{\alpha}$]-3x[^{12}C][a]

Label	Expno	Ω_I region / ppm	Observed signals	Ω_S region / ppm	Selected protons	Couplings extracted
SS25	C/1029	1.82-1.95	3x[$^{13}C^{\alpha}$] 3n[$^{13}C^{\beta}$]	1.43-1.53	7a[^{12}C]	3x[$^{13}C^{\alpha}$]-7a[^{12}C] 3n[$^{13}C^{\beta}$]-7a[^{12}C]
SS26	C/1030	1.55-1.64	5x[$^{13}C^{\alpha}$]	1.43-1.53	7a[^{12}C]	5x[$^{13}C^{\alpha}$]-7a[^{12}C][a]
SS27	C/1031	1.84-1.913	6x[$^{13}C^{\beta}$]	1.43-1.53	7a[^{12}C] 6n[$^{13}C^{\beta}$]	6x[$^{13}C^{\beta}$]-7a[^{12}C] 6x[$^{13}C^{\beta}$]-6n[$^{13}C^{\beta}$] [c]
SS28	C/1033	1.53-1.63	7a[$^{13}C^{\beta}$] 7s[$^{13}C^{\alpha}$]	1.9-2.1	3x[^{12}C]	7a[$^{13}C^{\beta}$]-3x[^{12}C] 7s[$^{13}C^{\alpha}$]-3x[^{12}C][a]
SS29	C/1034	1.82-1.95	3x[$^{13}C^{\alpha}$] 3n[$^{13}C^{\beta}$]	2.4-2.5	1[^{12}C]	3x[$^{13}C^{\alpha}$]-1[^{12}C] 3n[$^{13}C^{\beta}$]-1[^{12}C]
SS30	C/1035	1.55-1.64	5x[$^{13}C^{\alpha}$]	2.4-2.5	1[^{12}C]	5x[$^{13}C^{\alpha}$]-1[^{12}C][a]
SS31	D/1003	1.31-1.40	7a[$^{13}C^{\alpha}$]	1.53-1.63	7a[$^{13}C^{\beta}$] 7s[$^{13}C^{\alpha}$]	7a[$^{13}C^{\alpha}$]-7s[$^{13}C^{\alpha}$]
SS32	D/1005	1.84-1.913	6x[$^{13}C^{\beta}$]	1.69-1.766	3n[^{12}C] 5x[^{12}C]	6x[$^{13}C^{\beta}$]-3n[^{12}C][d] 6x[$^{13}C^{\beta}$]-5x[^{12}C] [e]
SS33	D/1006	1.415-1.525	5n[$^{13}C^{\beta}$] 6n[$^{13}C^{\beta}$]	1.62-1.68	7s[^{12}C]	5n[$^{13}C^{\beta}$]-7s[^{12}C] 6n[$^{13}C^{\beta}$]-7s[^{12}C]
SS34	D/1008	1.82-1.95	3x[$^{13}C^{\alpha}$] 3n[$^{13}C^{\beta}$]	2.05-2.20	3x[$^{13}C^{\beta}$]	3n[$^{13}C^{\beta}$]-3x[$^{13}C^{\beta}$]
SS35	D/1009	1.18-1.303	5n[$^{13}C^{\alpha}$] 6n[$^{13}C^{\alpha}$]	1.71-1.80	6x[^{12}C] 3n[^{12}C]	5n[$^{13}C^{\alpha}$]-3n[^{12}C] 5n[$^{13}C^{\alpha}$]-6x[^{12}C] [e]
SS36	D/1010	1.55-1.64	5x[$^{13}C^{\alpha}$]	1.71-1.80	6x[^{12}C] 3n[^{12}C]	5x[$^{13}C^{\alpha}$]-3n[^{12}C][a] 5x[$^{13}C^{\alpha}$]-6x[^{12}C] [e]
SS37	D/1011	1.415-1.525	5n[$^{13}C^{\beta}$] 6n[$^{13}C^{\beta}$]	1.65-1.77	3n[^{12}C] 5x[^{12}C] 6x[^{12}C] 7s[^{12}C]	6n[$^{13}C^{\alpha}$]-3n[^{12}C] 6n[$^{13}C^{\alpha}$]-5x[^{12}C] 6n[$^{13}C^{\alpha}$]-7s[^{12}C] [f]
SS38	D/1012	1.84-1.913	6x[$^{13}C^{\beta}$]	1.715-1.765	3n[^{12}C] 5x[^{12}C][g]	6x[$^{13}C^{\beta}$]-3n[^{12}C] 6x[$^{13}C^{\beta}$]-5x[^{12}C] [g]

[a] No splitting was observed, meaning the coupling was assigned a value of 0 Hz.

[b] The 3n[$^{13}C^{\alpha}$] multiplet was only partly irradiated. The 3x[$^{13}C^{\alpha}$] response turns out not visible.

[c] Both couplings evolve, implying a doublet of doublet is expected. Since the spectral window in F_1 was 5 Hz, the 6x[$^{13}C^{\beta}$]-6n[$^{13}C^{\beta}$] splitting is folded.

[d] Splitting not observed due to insufficient digital resolution in F_1.

[e] Both couplings evolve, implying a doublet of doublet is expected.

[f] All three couplings evolve, implying a doublet of doublet of doublet is expected. Only a doublet of doublet is found with the expected values of 6n[$^{13}C^{\alpha}$]-5x[^{12}C] and 6n[$^{13}C^{\alpha}$]-7s[^{12}C], meaning the 6n[$^{13}C^{\alpha}$]-3n[^{12}C] splitting is assigned a value of 0 Hz.

[g] The 5x[^{12}C] multiplet was only partly irradiated, meaning the response is a mixed response of a 6x[$^{13}C^{\beta}$]-3n[^{12}C] doublet and a 6x[$^{13}C^{\beta}$]-3n[^{12}C] + 6x[$^{13}C^{\beta}$]-5x[^{12}C] doublet of doublet. The 6x[$^{13}C^{\beta}$]-3n[^{12}C] coupling could be measured on the former.

5.3 Coupling data

Table S12: *J*-coupling data for norcamphor.

Values affected by the effects of strong coupling are shown in red.
*Strongly coupled protons in the all-^{12}C isotopomer are shaded **pink**.*
Previously reported J-coupling values measured in $CDCl_3$ by Marshall and Walter are shown.
[10] These were derived using spectral simulation on partly deuterated forms of norcamphor.
Note that they reported coupling signs, while the selective 2DJ spectra in this work only provide coupling magnitudes. Values deviating by at least 0.5 Hz from the Marshall values are shaded green, while newly found nonzero couplings smaller than 0.5 Hz are shaded blue.

Coupling partners		J / Hz					
		PSYCHEDELIC		SERFBIRD/SATASERF		Final coupling	Marshall
1	3n	--	--	0.5 SS29	--	**0.5**	0.0
1	3x	0.9 P1	0.9 P3	0.9 SS29	1.0 SB2	**1.0**	0.0
1	4	1.2 P1	1.3 P4	--	1.3 SB1	**1.3**	1.2
1	5n	--	--	0.3 SS13	0.3 SS15	**0.3**	-0.3
1	5x	--	--	0.0 SS30	--	**0.0**	0.2
1	6n	--	--	0.6 SS13	0.6 SS15	**0.6**	0.1
1	6x	4.8 P1	--	4.9 SS7	--	**4.9**	4.7
1	7a	1.2 P1	1.2 P2	1.2 SS17	--	**1.2**	1.2
1	7s	1.6 P1	--	1.6 SS17	--	**1.6**	1.6
3n	3x	17.6 P3	--	17.6 SS34	--	**17.6**	-17.6
3n	4	--	--	0.5 SS22	--	**0.5**	0.0
3n	5n	--	--	0.3 SS35	--	**0.3**	0.0
3n	5x	--	--	0.0 SS36	--	**0.0**	0.0

Coupling partners		J / Hz					
		PSYCHEDELIC		SERFBIRD/SATASERF		Final coupling	Marshall
3n	6n	--	--	0.0 SS37	--	**0.0**	0.0
3n	6x	--	--	0.3 SS38	--	**0.3**	0.0
3n	7a	4.3 P2	--	4.3 SS25	--	**4.3**	4.2
3n	7s	--	--	0.0 SS23	--	**0.0**	0.0
3x	4	4.7 P3	4.7 P4	4.7 SS22	4.7 SB2	**4.7**	4.8
3x	5n	--	--	0.4 SS24	--	**0.4**	0.0
3x	5x	2.7 P3	--	2.8 SS9	--	**2.8**	2.3
3x	6n	--	--	0.0 SS24	--	**0.0**	0.0
3x	6x	0.8 P3	--	1.0 SS18	--	**1.0**	0.0
3x	7a	--	--	0.4 SS25	0.4 SS29	**0.4**	0.0
3x	7s	--	--	0.0 SS27	--	**0.0**	0.0
4	5n	--	--	0.6 SS12	0.6 SS14	**0.6**	0.1
4	5x	4.1 P4	--	4.3 SS8	--	**4.3**	4.3
4	6n	--	--	0.3 SS12	0.4 SS14	**0.3**	-0.5
4	6x	--	--	0.6 SS11	--	**0.6**	0.7
4	7a	2.1 P2	2.1 P4	2.1 SS16	--	**2.1**	2.1
4	7s	1.6 P4	--	1.6 SS16	--	**1.6**	1.6
5n	5x	--	--	12.0 SS4	--	**12.0**	-12.8
5n	6n	--	--	9.1 SS1	9.0 SS2	**9.1**	9.1
5n	6x	--	--	4.5 SS5	4.5 SS35	**4.5**	4.7
5n	7a	--	--	0.0 SS20	--	**0.0**	-0.1

Coupling partners		J / Hz					
		PSYCHEDELIC		SERFBIRD/SATASERF		Final coupling	Marshall
5n	7s	--	--	2.2 SS10	2.2 SS33	**2.2**	2.1
5x	6n	--	--	4.3 SS6	--	**4.3**	4.6
5x	6x	--	--	12.0 SS32	12.0 SS36	**12.0**	12.1
5x	7a	--	--	0.0 SS26	--	**0.0**	0.0
5x	7s	--	--	0.0 SS21	--	**0.0**	0.0
6n	6x	--	--	12.6 SS3	--	**12.6**	-12.3
6n	7a	--	--	0.0 SS20	--	**0.0**	-0.1
6n	7s	--	--	2.2 SS33	--	**2.2**	2.0
6x	7a	--	--	0.0 SS27	--	**0.0**	0.0
6x	7s	--	--	0.0 SS19	--	**0.0**	0.0
7a	7s	10.1 P2	--	10.1 SS31	--	**10.1**	-10.2

6. References

(1) Enthart, A.; Freudenberger, J. C.; Furrer, J.; Kessler, H.; Luy, B. *J. Magn. Reson.* **2008**, *192*, 314-322.
(2) Foroozandeh, M.; Adams, R. W.; Meharry, N. J.; Jeannerat, D.; Nilsson, M.; Morris, G. A. *Angew. Chem. Int. Ed.* **2014**, *53*, 6990-6992.
(3) Sinnaeve, D.; Ilgen, J.; Di Pietro, M. E.; Primozic, J. J.; Schmidts, V.; Thiele, C. M.; Luy, B. *Angew. Chem. Int. Ed.* **2020**, *59*, 5316-5320.
(4) Kupce, E.; Boyd, J.; Campbell, I. D. *J. Magn. Reson. Ser. B* **1995**, *106*, 300-303.
(5) Sinnaeve, D. *Magn. Reson. Chem.* **2018**, *56*, 947-953.
(6) Castañar, L.; Nolis, P.; Virgili, A.; Parella, T. *Chem. Eur. J.* **2013**, *19*, 17283-17286.
(7) (a) Kiraly, P.; Nilsson, M.; Morris, G. A. *Magn. Reson. Chem.* **2018**, *56*, 993-1005; (b) Kiraly, P.; Morris, G. A.; Liu, Q. X.; Nilsson, M. *Synlett* **2019**, *30*, 1015-1025.
(8) (a) Kaltschnee, L.; Kolmer, A.; Timari, I.; Schmidts, V.; Adams, R. W.; Nilsson, M.; Kover, K. E.; Morris, G. A.; Thiele, C. M. *Chem. Commun.* **2014**, *50*, 15702-15705; (b) Reinsperger, T.; Luy, B. *J. Magn. Reson.* **2014**, *239*, 110-120.
(9) McIntyre, D. D.; Vogel, H. J. *J. Nat. Prod.* **1989**, *52*, 1008-1014.
(10) Marshall, J. L.; Walter, S. R. *J. Am. Chem. Soc.* **1974**, *96*, 6358-6362.